Nuclear Instruments and Methods in Physics Research A 620 (2010) 147–154

Contents lists available at ScienceDirect

Nuclear Instruments and Methods in Physics Research A

journal homepage: www.elsevier.com/locate/nima

Effects of external magnetic fields on the operation of high-gradient accelerating structures

Diktys Stratakis *, Juan C. Gallardo, Robert B. Palmer

Department of Physics, Brookhaven National Laboratory, Upton, NY 11973, USA

ARTICLE INFO

Article history:
Received 28 February 2010
Accepted 31 March 2010
Available online 14 April 2010

Keywords:
Accelerator physics
High-gradient accelerating structures
RF breakdown
Muon collider

ABSTRACT

Field emission in an rf cavity in the presence of external magnetic fields is examined. We show that emitted electrons from a sharp protrusion are focused by the magnetic field into small spots at another location in the cavity where they heat its surface. Scaling laws are established for the beam's induced heat in terms of macroscopic quantities such as magnetic field, accelerating gradient and spot dimensions. We find that when the magnetic field is of the order of a Tesla, the induced thermal stresses by the pulsed electron flux exceed the elastic limit and the surface becomes prone to cycling fatigue. The implication of these findings on the observed surface damage and magnetic-field-depended breakdown of an 805 MHz cavity is addressed.

1. Introduction

Much effort is underway to explore the feasibility of designing and constructing a high-luminosity muon-collider [1] and neutrino factory [2]. In these designs, ionization cooling [3] reduces the emittance of the muon beam as it passes through an absorber, thereby lowering the muons transverse- and longitudinal-momenta. Thereafter, longitudinal momentum is restored by accelerating the beam through an rf cavity (typically 201–805 MHz), leaving a net loss of the transverse momentum. The net effect of ionization cooling is more efficient when a solenoid strongly focuses the beam through the absorber [4]. Because the field lines extend beyond the solenoid, the rf cavities contain significant magnetic fields. Thus, it is of fundamental importance that we understand thoroughly the operation of the rf cavities under external magnetic fields.

Three recent major experiments at the MuCool Test Area (MTA) [5] at Fermi National Laboratory tested the efficiency of the rf cavities within magnetic fields: one with a multi-cell 805 MHz cavity, and two with a "pillbox" 201 and 805 MHz [6]. All experiments have shown that cavities suffer damage and/or reduced operating gradients when exposed to the external fields. Importantly, they suggested that the operational problems were associated with the combined effect of unwanted emission of electrons from locally enhanced field regions [7,8], and the presence of external magnetic fields [9].

Our work was motivated, in part, by Moretti's experimental observation [6] of a 60% reduction of the maximum accelerating gradient in the "pillbox" cavity in the presence of uniform, axial, external magnetic fields. Palmer et al., [10] related this lessening of the gradient to the existence on the cavity's surface of microscopic roughnesses, or *asperities*, greatly enhancing the local electric field. Their model suggested that dark current electrons from an asperity are accelerated by the rf fields, and in the presence of a sufficiently strong magnetic field ($B \approx 0.5$ T), are focused into small spots at another location in the cavity where they heat the surface and thus, might initiate breakdown [11–13]. The three interesting questions then are how those emitted electrons raise the temperature, whether this effect alone is sufficient to create surface damage, and, how this temperature rise scales with the external magnetic field. A key requirement to resolve these issues is the ability to simulate field emission from locally enhanced field regions in rf cavities under external magnetic fields.

The intent of our present work is to develop a methodology to estimate the rise in temperature from field-emitted electrons arising from a sharp protrusion where the electric field is intense. We use a simple model to address this issue, the analysis of which yields interesting information on the electron impact energy, on the mechanism that initiates damage in rf cavities within the external magnetic fields, and on the required magnetic field strength over which the surface becomes prone to fatigue.

We report the findings from our simulations modeling Moretti's "pillbox" experiment [6] (PB) and provide crucial information on operating the 805 MHz cavity under differently configured magnetic fields and intensities of emission currents that likely will be important in designing and predicting the outcomes in future lattices of the muon collider and neutrino factory. We emphasize that our simulation fully incorporated the effect of both rf and locally enhanced fields caused by microscopic

* Corresponding author.
E-mail address: diktys@bnl.gov (D. Stratakis).

0168-9002/$ - see front matter © 2010 Elsevier B.V. All rights reserved.
doi:10.1016/j.nima.2010.03.167

asperities. Furthermore, we also considered space-charge effects into our analysis. We demonstrate that cyclic heating from the repeated bombardment of dark current electrons may damage the surface of the 805 MHz cavity; such degradation might contribute to its eventual breakdown. The theory is simple and intuitive, and agrees adequately with earlier experimental data.

The outline of this paper is as follows: in Section 2 we review our emission model and our simulation parameters. In Section 3 we detail the tracks of particles within the "pillbox" cavity under external magnetic fields. In Section 4, we estimate the induced temperature rise and discuss some physical insights from our results. Finally, we present our conclusions in Section 5.

2. Emission model and simulation parameters

In this section, we will review the parameters we used in our simulation and discuss the similarities and differences with the ones measured in related experiments.

The MTA at Fermilab earlier designed a multi-cell cavity as a part of their cooling studies for a future neutrino factory and muon collider [14]. It consisted of six open 805 MHz rf cavities with vacuum windows at their ends [15]. The cavity was tested in the presence external magnetic fields, and, after some time, damage spots were observed on one of the cavity's windows, which was a clear evidence of dark-current electrons impinging there. Detailed measurements [6,15] of those currents showed that they scaled as a power law with the cavity's electric field which suggested that the field-emission follows the Fowler–Nordheim (FN) relation [16]

$$J = 6.0\times10^{-12}\frac{\beta_e^{2.5}G^{2.5}}{\phi^{1.75}}10^{4.52\phi^{-0.5}}(e^{-(6.53\times10^9\phi^{1.5}/\beta_eG)}), \tag{1}$$

where J is the average current density in an rf cycle in A/m^2, G the electric field on the cavity's surface in V/m, ϕ the metal's work function in eV, and β_e the enhancement factor, defined as the maximum local electric field divided by the average surrounding surface field. According to the FN model, electrons are emitted from small point sources where the local electric fields ($G_l=\beta_eG$) are large enough to pull electrons out of the metal by barrier tunneling.

In the MTA's multi-cell experiment, the location of the window damage corresponded to a magnetically focused dark current coming from one of the high-field irises. Studies of the internal surface of the cavity showed [6], in fact, sharp cone protrusions (microscopic asperities) along the cavity's iris, which may explain the expected enhancement of the local field at that location. The net measured [15] emission current was 100 mA when the surface gradient was $\approx$50 MV/m and the average surface area of each emitter was 10^{-14} m^2.

In our simulation, we model each individual emitter (asperity) as a prolate spheroid, an approximation that is not far from the actual shape of the asperity, as indicated by recent microscopic images along the cavity's surface [17]. The advantage of our approach is that then we know analytically the behavior of the electric field. Specifically, in terms of the prolate spheroidal coordinates (u,v), defined by $z=c_2uv$, $R=c_2[(u^2-1)(1-v^2)]^{1/2}$ the expression for the potential becomes [18]

$$V(R,z) = Gz\left(1-\frac{\coth^{-1}u-1/u}{\coth^{-1}u_0-(1/u_0)}\right) \tag{2}$$

where $u_0=\alpha/(\alpha^2-b^2)^{1/2}$, G the cavity surface field, α the major axis of the prolate spheroid, and b its minor axis. Then, near the asperity region the electric fields along the normal- and transverse-directions are described by the following relations [19]:

$$G_{R,ASP}(R,z) = -\frac{\partial V}{\partial R} = \left[\frac{z}{\left(\coth^{-1}u_0-(1/u_0)\right)}\frac{1}{u^2(1-u^2)}\left[1+\frac{1+\frac{r^2}{c_2^2}}{\sqrt{\frac{r^4}{c_2^4}+\frac{2(R^2-z^2)}{c_2^2}+1}}\right]\frac{R}{c_2^2u}\right]G \tag{3}$$

and

$$G_{z,ASP}(R,z) = -\frac{\partial V}{\partial z} = -\left[\left[1-\frac{\coth^{-1}u-(1/u)}{\coth^{-1}u_0-(1/u_0)}\right] - \frac{z}{\left(\coth^{-1}u_0-(1/u_0)\right)}\frac{1}{u^2(1-u^2)}\left[1-\frac{\frac{r^2}{c_2^2}-1}{\sqrt{\frac{r^4}{c_2^4}+\frac{2(R^2-z^2)}{c_2^2}+1}}\right]\frac{z}{c_2^2u}\right]G \tag{4}$$

where $r=\sqrt{R^2+z^2}$ and $c_2=(a^2-b^2)^{1/2}$. Next, to calculate the net cavity field, we superimpose the asperity enhanced fields on the actual rf fields (lacking asperity)

$$G_R(R,z) = G_{R,ASP}(R,z)+G_{R,RF}(R,z), \tag{5}$$

and

$$G_z(R,z) = G_{z,ASP}(R,z)+G_{z,RF}(R,z). \tag{6}$$

To facilitate a more detailed comparison between experiment and theory, in our simulation we assumed that the emission from the asperities is governed by the FN model by using the aforementioned measured parameters from the MTA. We chose $a=62$ μm and $b=1.77$ μm for the asperity's major- and minor-axis, respectively. Fig. 1 is a detailed illustration of the emitter's shape [Fig. 1(a)] and of the emitted current along the asperity major axis [Fig. 1(b)]. Note that the emitted current is obtained using the integral

$$I = \int JdA, \tag{7}$$

where J is the average current density from Eq. (1), and dA the surface area which is given by $dA=2\pi R\sqrt{1+\left(\frac{dR}{dz}\right)^2}dz$.

To highlight the similarities between our simulation parameters and the actual measurements, by carefully examining Fig. 1 we note the following points. The current is nonzero in a very short region along the tip, approximately equal to the radius of curvature, which is defined by $r_c=b^2/\alpha$ and for our case is 0.05 μm. Thus, the emitter surface area becomes $\approx10^{-14}$ m^2, which is consistent with the experimental findings. Additionally, the net current value in our simulation is of the order of 100 mA, also agreeing well with the measured value.

3. Electron motion in a cavity

In Ref. [10] Palmer et al. tracked single electrons within 201 and 805 MHz cavities. They found the following: emitted electrons from one side of the cavity were accelerated by the rf fields, and struck another location in the rf cavity with high energies ($\approx$1 MeV). In the absence of magnetic fields, these impacts were spread over large areas and did not harm the cavity's surface. However, with higher magnetic fields ($B\approx0.5$ T) the very energetic electrons were focused into small spots, suggesting that the induced temperature rise from the collision was sufficient to generate material damage that, in turn, might

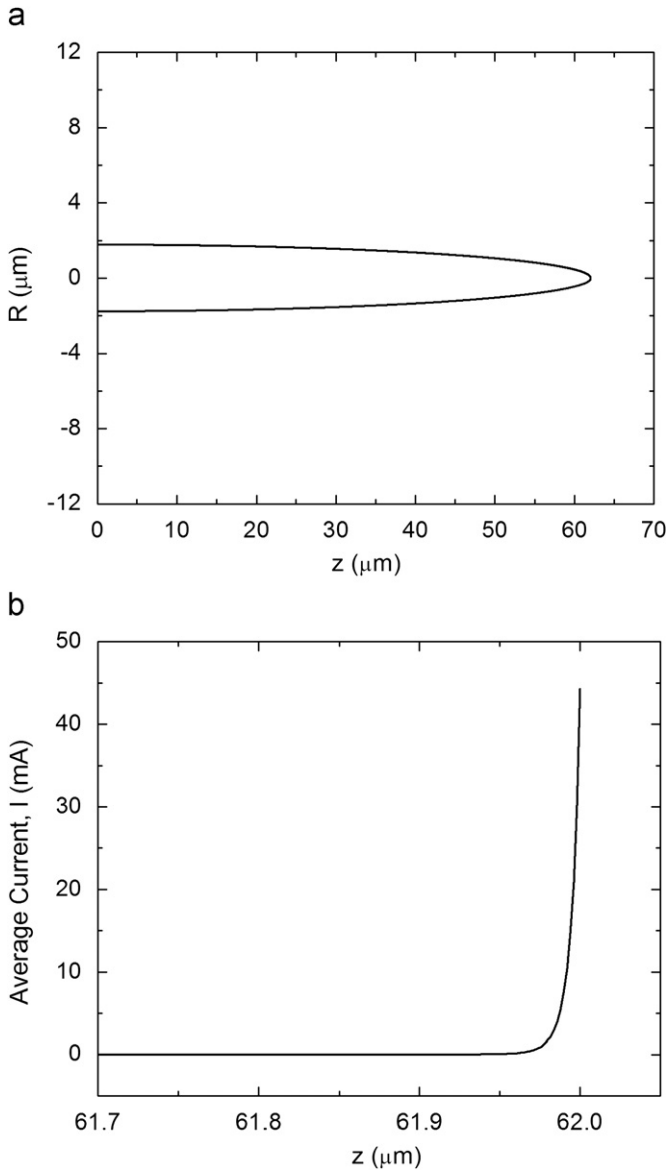

Fig. 1. Asperity simulation model: (a) Asperity shape and size and (b) emission current along the asperity major-axis. The assumed field enhancement was $\beta_e \approx 375$.

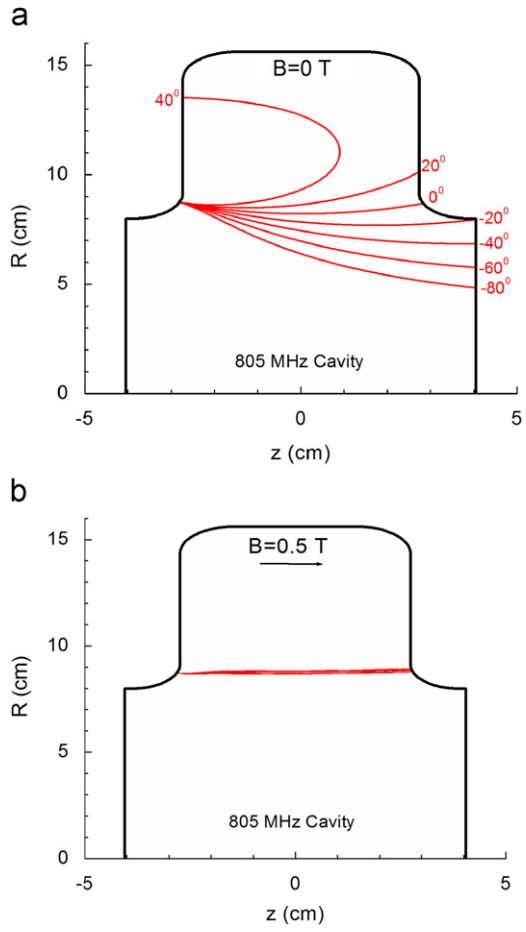

Fig. 2. Trajectories of electrons field emitted at different rf phases as found in Ref. [10]: (a) with no external magnetic field and (b) an axial magnetic field of 0.5 T.

limit the cavity's operation. Fig. 2 summarizes the aforementioned observations in Ref. [10].

However, their study left several unanswered questions. First, the simulations were restricted to following single particles. How will a beam's distribution evolve, and how will space-charge influence its transport? Second, their previous simulations assumed that the beam was emitted from flat surfaces. What can we learn if we track electrons from asperities that resemble more closely the conditions of the relevant experiments? Third, what is the predicted temperature rise from dark currents? Fourth, will that increase be enough to damage the cavity, and how does it scale with the external magnetic fields?

In addressing these questions, we tracked electrons from the asperities described in Section 2. To better relate our findings with that of the PB experiment, in our simulations we assumed a "pillbox" 805 MHz cavity identical to that described in Ref. [6]. Details about the cavity's design parameters are given elsewhere [20]. To perform the simulations, we used PARMELA [21], a tracking code developed at Los Alamos National Laboratory that fully incorporates space-charge effects. PARMELA tracked the particles along a grid that used a superposition of the analytically calculated asperity fields and rf fields (lacking asperity) that were generated by SUPERFISH [22]. For simplicity, the asperity was placed along the cavity's axis [see Fig. 3(a)] and the external magnetic field, B, was uniform, and pointing along the z-direction.

Fig. 3 depicts the pillbox cavity used in our simulation, and the beam distribution at different positions. In the simulation, each particle was launched perpendicular to the surface with initial energy of 1 eV. For this example we assume $B=0.9$ T and $G=40$ MV/m. The data in Fig. 3 may be interpreted as follows. We note that the distribution is initially enclosed within a very narrow region approximately equal to the radius of curvature (i.e. 50 nm). Physically, we expected this distribution because the current becomes negligible outside that area [see Fig. 1(b)]. Because the initial energy of the beam is low as it leaves the source, strong repelling space-charge forces are present that, in combination with the asperity radial fields, give transverse momenta to the emitted electrons causing an increase in the beamlet's radius [middle in Fig. 3(b)]. However, at distances far from the source, the space-charge becomes negligible, and thereafter, each particle moves only under the influence of the external applied fields; in our case, the external magnetic field and the rf fields. If the magnetic field exceeds 0.5 T, the beam is finally focused as a small spot on the opposing cavity wall [see right in Fig. 3(b)]. In the next subsections, we will examine the dependence of the final beamlet radius, R_f, on the magnetic field (Section 3.1), and on the beam's current (Section 3.2) for selected values of G and B that correspond to typical operating parameters

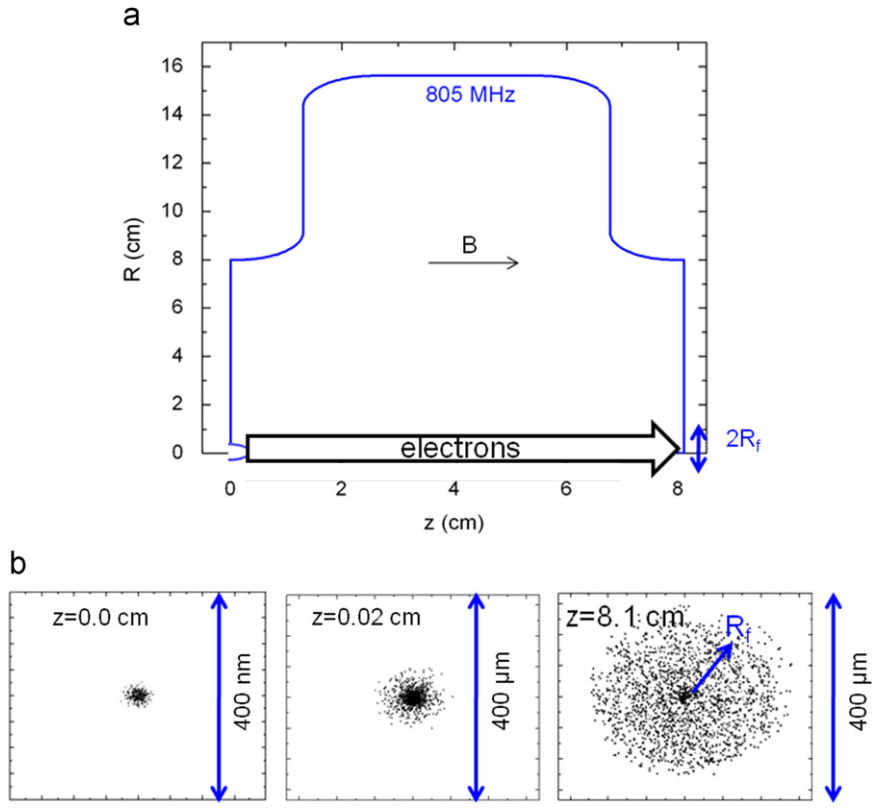

Fig. 3. (a) The 805 MHz pillbox rf cavity used in our simulation. The asperity was placed along the cavity's axis ($R=0$, $z=0$). Distances are not to scale and (b) beam distribution at $z=0$ cm (asperity), $z=0.02$ cm, and at $z=8.1$ cm (cavity wall). The magnetic-field strength was 0.9 T and pointed along the z-direction. The black arrow shows the direction of the field emitted electrons as they get accelerated by the rf fields and finally focused by the external magnetic field into the opposing side of the cavity.

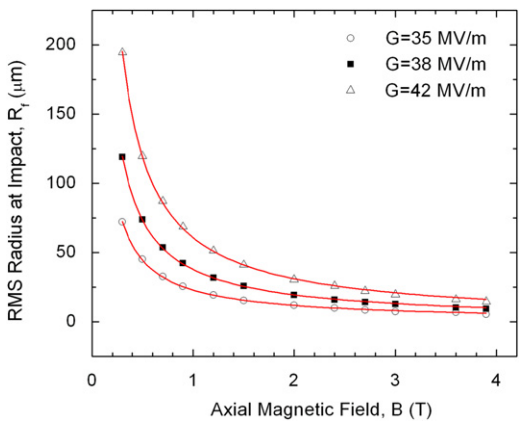

Fig. 4. Final beamlet radius versus magnetic field for different surface gradients.

used in the PB experiment. Then, we estimate the deposited power density on the cavity's surface (Section 3.3).

3.1. Beamlet radius with magnetic field

Fig. 4 illustrates the beam's radius versus the magnetic field for three different accelerating gradients. For all cases, its radius displays a $1/B$ dependence on the magnetic field. Furthermore, as the gradient becomes larger, the size of the beamlet increases. We believe that this is because of the higher currents associated with those gradients [see Eq. (1)]. Consequently, the repelling space-charge force becomes stronger, eventually leading to larger beamlets.

3.2. Beamlet radius with current

If there were no asperity and the rf field is perpendicular to the surface, then for emission from a small area, space-charge forces give transverse momenta to electrons causing the beam radius to increase. As the beam radius increases and the electrons are accelerated then space-charge forces become weaker and it has been shown [10] that the rms beamlet radius scales with the beam current I as

$$R \propto \frac{\sqrt{I}}{B}. \tag{8}$$

where B is the magnetic field. We note that the above expression indicates a $1/B$ dependence of the radius, a result consistent with the findings in Section 3.1.

To test the accuracy of Eq. (8) for our case, we undertook a PARMELA simulation within the 805 MHz cavity under a constant external magnetic field. By assuming a planar emitter (no asperity) at $z=0$, we systematically varied the beam's current and each time recorded the beamlet's radius, R_f, at the point where the beam impacts the opposing wall (see Fig. 5(a)). A fit to the data revealed indeed that $R_f \propto \sqrt{I}/B$. However, if electrons are emitted from the tip of an asperity, they first will spread due the transverse momentum they receive from the local radial electric fields; hereby, the effect of space-charge is reduced. To illustrate this expectation, we replaced the flat emitter by the asperity shown Fig. 1, and repeated the simulation. A fit to the data revealed now that the beamlet's radius scales as

$$R_f = C_2 \frac{I^j}{B}, \tag{9}$$

where j equals 0.33. If R_f is expressed in μm, B in T, and I in μA, then C_2 equals 22.6. We point out the persistence of the $1/B$

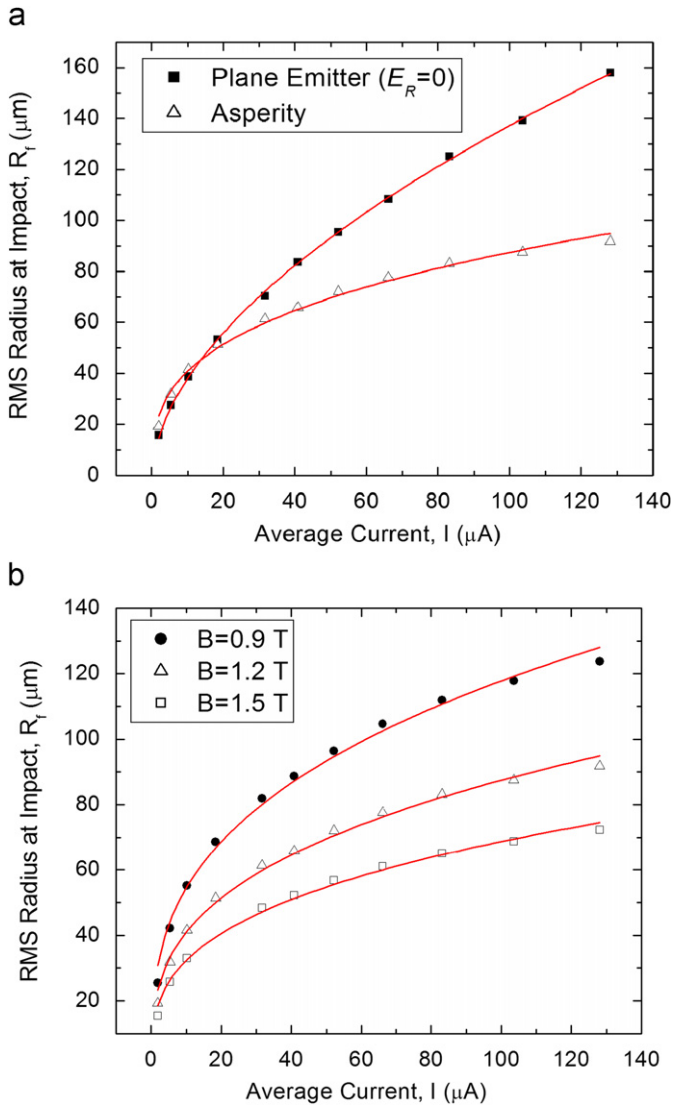

Fig. 5. (a) Final beamlet radius versus current for a planar emitter (black squares), and for an asperity (white triangles). The external field was 1.2 T and (b) final radius of the beamlet for an asperity emitter at three different magnetic field strengths: B=0.9, 1.2, and 1.5 T.

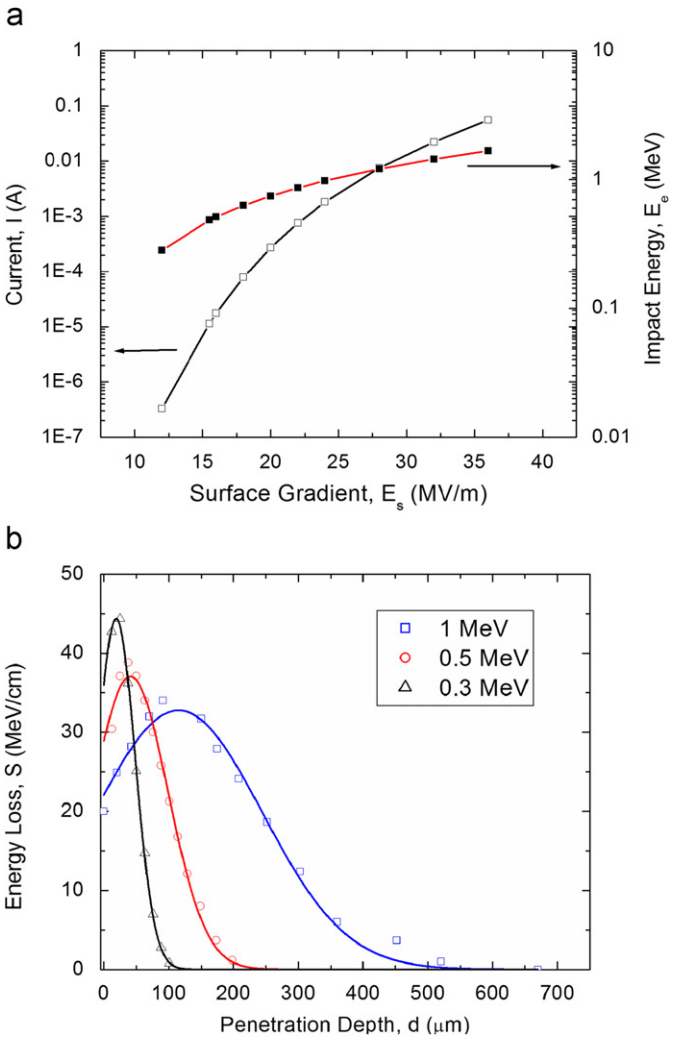

Fig. 6. (a) The simulated final impact electron energy and emission current as a function of axial gradient for the pillbox cavity and (b) Cu-stopping powers versus penetration depth for three different impact electron energies. The solid lines are fits of a Gaussian function to the experimental data.

dependence with the field. We also emphasize that the result shown in Eq. (9) is weakly dependent on the asperity's dimensions and the external magnetic fields (assuming that β_e is not changing). The latter conclusion is illustrated in Fig. 5(b) where Eq. (9) was repeatedly reproduced for three different strengths of magnetic fields.

3.3. Deposited energy at the cavity surface

As the beam approaches the far side of the cavity, its surface is continuously bombarded by electrons. The impact energy and emission current as a function of the accelerating gradient for the 805 MHz cavity is shown in Fig. 6(a). The power per unit area of the electron beam hitting the surface is given by

$$W_s = \frac{P}{(\pi R_f{}^2)}, \tag{10}$$

were P is the incident power, and R_f the rms beamlet's radius. As those electrons penetrate the metal, they gradually lose energy in many small steps. Both the penetration depth and the energy loss per unit length (stopping power) depend on the properties of the material the beam passes through, as well as the incident energy. The stopping power $S=-dE/dz$, for different incident energies and materials, has been measured and recorded in databases [23]. Using this information in Fig. 6(b), we examine the electron-penetration depth for three typical operational acceleration gradients of the 805 MHz pillbox cavity. We assume a Cu surface with physical properties shown in Table 1. Note that the dots are experimental data adopted from Ref. [23] and the solid lines are Gaussian fits to the data. The plots may be interpreted as follows. Higher values of rf accelerating gradients imply a larger value of the electron energy at impact with the wall and therefore a larger value of the penetration depth as shown in Fig. 6. For incident kinetic energies $E_e<0.5$ MeV, the penetration depth reduces and the stopping power increases more steeply reaching a maximum, close to the surface boundary.

As the electrons penetrate inside Cu they deposit energy and the cavity's temperature rises. Previously conducted simulations [24] revealed that the majority of energy is deposited within a cylinder-like region with radius R_f and length equal to the penetration depth. Then, the heat generated by unit volume can

Table 1
Physical parameters of Cu

Density, ρ (g/cm^3)	8.96
Specific heat, C_s (J/g—°C)	0.385
Thermal conductivity, K_{th} (W/cm—°C)	4.01
Thermal diffusivity, α_d (cm^2/s)	1.16
Atomic number, Z	29
Atomic weight, A	63.5

be approximated by

$$W=\frac{I}{q(\pi R_f{}^2)}\frac{dE}{dz}\propto\frac{B^2}{q(\pi I^{2j-1})}\frac{dE}{dz} \tag{11}$$

where $P=E_eI/q$, q is the charge of an electron, and dE/dz the stopping power which is a Gaussian fit to the data in Fig. 6(b).

By carefully examining Eq. (11) the following points are noteworthy. First, the delivered power density increases with the gradient. Since power depends on the beam's current, this fact is a direct consequence of the exponential dependence of current with gradient from the FN expression in Eq. (1). Second, and more importantly, although an external magnetic field does not modify the incident beam's energy or net current, it can substantially increase the density of the surface-deposited power. The increase of W with B, shown in Eq. (11), was anticipated simply because of the smaller size of the beam, R_f, associated with the strong focusing of the magnetic field. As we show in the next section, this fact may be the primary cause of the severe problems incurred when operating rf in external magnetic fields.

4. Surface temperature rise model

On impact with the cavity surface, the incident beam releases heat as it penetrates through the metal. We shall consider that our source is a cylinder with a radius equal to the spot size R_f, and length of the penetration depth, D. Then, the heat generated per unit volume, W, can be approximated by Eq. (11) and the induced temperature rise on the cavity's surface can be determined by using the heat conduction in cylindrical coordinates

$$\frac{1}{R}\frac{\partial}{\partial R}\left[R\frac{\partial T}{\partial R}\right]+\frac{\partial^2T}{\partial z^2}+\frac{1}{K_{th}}W(R,z,t)=\frac{\rho C_s}{K_{th}}\frac{\partial T}{\partial t}, \tag{12}$$

where K_{th} is the thermal conductivity, ρ the material's density, C_s the specific heat, and τ_{add} the duration of rf pulse. We can reduce the heat conduction equation to an integral using Green's functions [25]

$$\Delta T=\frac{\alpha_d}{K_{th}}\int_0^{\tau_{add}}\int_0^{D}\int_0^{R_f}G_{Rz}W(R',z',t')2\pi R'\,dR'\,dz'\,dt' \tag{13}$$

where D is the penetration depth, a_d the thermal diffusivity, and G_{Rz} the Green function. For simplicity when writing Eq. (13) we assumed that the temperature depends on coordinates R and z only. For this case G is the product of the two-one dimensional Green functions [26]

$$G_z(z,t|z',t')=\frac{1}{\sqrt{4\pi\alpha_d(t-t')}}\left[e^{-\frac{(z-z')^2}{4\alpha_d(t-t')}}+e^{-\frac{(z+z')^2}{4\alpha_d(t-t')}}\right] \tag{14}$$

and

$$G_R(R,t|R',t')=\frac{1}{4\pi\alpha_d(t-t')}e^{-((R^2+R^2)/4\alpha_d(t-t'))}I_0\left[\frac{RR'}{2\alpha_d(t-t')}\right] \tag{15}$$

where I_0 is the modified Bessel function of the first kind. By combining Eqs. (11), (14), and (15), Eq. (13) becomes

$$\Delta T=\frac{2\alpha_d}{qK_{th}R_f^2}\times\int_0^{\tau_{add}}Idt'\left(\int_0^{R_f}dR'\frac{1}{4\pi\alpha_d(t-t')}R'e^{-\frac{R^2+R'^2}{4\alpha_d(t-t')}}I_0\left(\frac{RR'}{2\alpha_d(t-t')}\right)\right)\times\left(\int_0^{D}dz'\frac{1}{\sqrt{4\pi\alpha_d(t-t')}}\left[e^{-\frac{(z-z')^2}{4\alpha_d(t-t')}}+e^{-\frac{(z+z')^2}{4\alpha_d(t-t')}}\right]\frac{dE}{dz'}\right) \tag{16}$$

From Eq. (16) it becomes apparent that the temperature strongly depends on the magnetic field and current as well as the properties of the material.

Here, it is interesting to recall that in previous pulse-heating experiments [27–29] serious damage and breakdown was evident as Cu samples were heated at temperatures far lower than its melting point. The damage was due to plastic deformation from pulse heating by a high-power rf pulse. Mechanical stress is induced on the surface of the metal due the temperature rise ΔT. When ΔT is above a safe temperature, the mechanical stress grows large enough to exceed the elastic limit (yield strength) and creates microscopic damages in the metal. The damage accumulates with each succeeding pulse and the cavity surface is destroyed after certain number of pulses. According to Musal [30] the approximate safe value is, $\Delta T_s=2\frac{(1-\nu)\sigma_t}{E\alpha_{th}}$, where ν is the Poisson ratio, E the elastic modulus, σ_t the yield stress, and α_{th} the coefficient of linear expansion. For Cu [28] $\alpha_{th}=1.65\times10^{-5}$/°C, $E=1.31\times10^{11}$ N/m^2, $\sigma_t=6.2\times10^7$ N/m^2, $\nu=0.33$ and a safe pulse heating temperature is $\Delta T_s\approx40$ °C. Interestingly, both pulse heating experiments at SLAC [27,28] and CERN [31] revealed significant cavity damage when heated above ΔT_s. However, the required temperature for surface fracture was found to be depending on the number of pulses n, and pulse length τ, and was approximately given by [32] $\Delta T_d=\left(\frac{1}{\zeta\sqrt{\tau}}\right)^{1/2}\sqrt{\ln(\frac{C}{n}+1)}$ with $C=1$ and $\zeta=5.0016\times10^{-14}$ if τ is in ns.

SLAC, considered pulse heating caused by the eddy currents created by a high-powered rf pulse. In this study, we consider the possibility that a similar phenomenon of metal destruction can occur by our pulsed electron flux. Next, we intend to estimate the temperature rise for which metal destruction due plastic

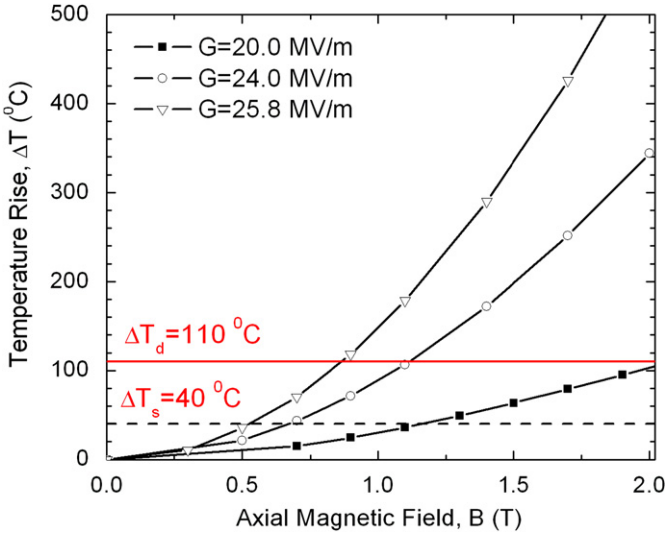

Fig. 7. Predicted temperature rise for the 805 MHz cavity in Ref. [6].

deformation occurs in the pillbox cavity. For the pillbox, $\tau=20$ μs, $n\approx 10^7$ and thus from the above equation we get $\Delta T_d \approx 110$ °C. Using Eq. (16) we estimate the temperature rise for the 805 MHz pillbox for different magnetic fields and accelerating gradients corresponding to the typical operational parameters of the PB experiment; our results are summarized in Fig. 7. For simplicity we restrict our calculation at the cavity surface so we set $z=0$ and $R=0$. The dashed line indicates the "safe" operating temperature, ΔT_s, and the solid line shows the temperature, ΔT_d where destruction is expected to occur. A glance at the figure indicates that at high gradient, the temperature rises rapidly as the magnetic field increases, a direct consequence of the focusing effect of the magnetic field. We notice from Fig. 4 that increasing the magnetic field reduces the beam's size. Thus, at high fields, the power density becomes greater, and consequently, the temperature rises. Fig. 7 also suggests that when the magnetic field is of the order of a Tesla, the temperature rise on Cu is enough to induce stress that is larger than its elastic limit. Consequently, the material becomes prone to cyclic fatigue beyond that point.

Shown in Fig. 8 are the predictions of our model for the required gradients G_s, G_d to raise the surface temperature at ΔT_s and ΔT_d, respectively, for a given magnetic field. The crosses denote the measured maximum accelerating gradients for different magnetic fields in the PB experiment in Ref. [6]. Notice that G_s, G_d scale with the magnetic field similar to the experimental data. Here it is interesting to recall that severe damage on the cavity's Cu surface was observed during the experiment, and this damage worsened as the strength of the magnetic field was increased. The experimental data lie much below the curves corresponding to the melting temperature of Cu (1085 °C), which suggests to us that a different mechanism (other than melting) is responsible for the observed damage and breakdown. The fact that the measurements tend to match G_d, the required gradient for surface degradation by pulse heating, indicates that the severe surface damage is likely associated to cyclic fatigue by the repeated bombardment of dark current electrons as they are focused strongly by the external magnetic field.

The data from the pillbox cavity experiment agree well with our model predictions for low fields, but tend to depart at large fields. There may be more than one cause for this behavior. Note that at higher fields ($B>2.5$ T) less time was spent for conditioning [6] and so the conditions at those fields likely were different from those assumed in our simulation. For instance, poor conditioning results in a higher field enhancement factor, β_e [13]. Thus, it is probable that β_e on three last data points will differ from those used in our simulation. Another possibility could be that the cavity was already severely damaged from the previous low field runs, a fact that may also modify β_e which was assumed constant in our simulation. An experimental program is currently underway to study these issues in detail. We stress, however, that our temperature calculation was an approximate one; our goal was to offer a lowest-order estimate and to propose simple scaling laws.

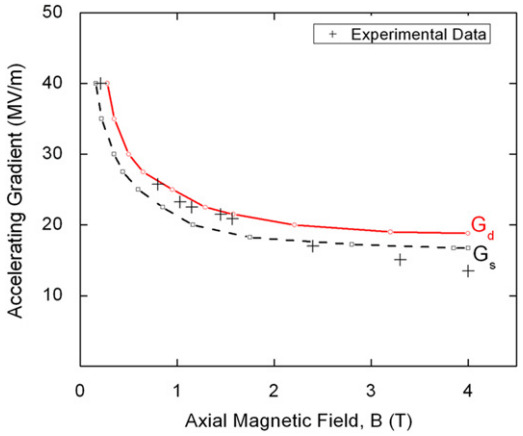

Fig. 8. Predictions of our model for the required accelerating gradients G_s, G_d for the 805 MHz cavity to reach the safe and surface-destruction temperature, ΔT_s and ΔT_d, respectively. Black crosses are measured breakdown data versus magnetic field from the PB experiment discussed in Ref. [6].

5. Conclusions

Recent experiments on the MTA revealed potentially serious problems for operating rf cavities in magnetic fields. Specifically, as the magnetic field was raised from 0 to 4 T, severe surface damage occurred in an 805 MHz rf cavity, accompanied by a 60% reduction of the maximum achievable accelerating gradient. Here, we detailed a simple model to describe the operation of rf cavities in magnetic fields. Our results suggest that the cause of damage in the 805 MHz cavity may be the impact of field-emitted electrons focused by the magnetic fields on to the cavity's copper surfaces. Such electrons would induce local cyclic heating of the cavity body. As in the SLAC experiment, the heated volume will be constrained by the surrounding unheated bulk material, and thus the surface will experience cyclic strain and fatigue.

While our preliminary analysis affords some quantification of the effects of the magnetic fields on the cavity's operation, we did not address other theoretical issues. For instance, we disregarded emission from secondary electrons, ignored the temperature dependence of material properties, we assumed that the magnetic field was uniform, and finally, we considered our analysis for one frequency: 805 MHz. On the theoretical level, it will be interesting to pursue additional simulations exploring these effects in more detail. Experimentally, there is a clear need for better designed experiments to study, systematically, the effect of external fields on the cavity's operation.

Nevertheless, our simple model yields the following conclusions: (a) In the presence of asperities, "dark current" electrons are field emitted, accelerated by the rf fields, and impact another location of the rf cavity. With a sufficient magnetic field ($B\sim 0.5$ T), the emitted electrons are focused into small spots; (b) the cavity surface temperature rises from the impact. This increase is a function of the rf accelerating gradient, and also depends on the magnetic field's strength and spots' sizes; (c) when $B\approx 1$ T the temperature rise is sufficient to induce stress to the surface that exceeds the elastic limit and thus the cavity becomes prone to cyclic fatigue; and, (d) numerical simulations suggest that the measured breakdown gradient of an 805 MHz pillbox cavity lie within, or close to the required gradient for surface destruction by pulse heating; thus, cyclic fatigue is likely the mechanism that contributes to the severe damage seen on the pillbox in the presence of magnetic fields.

Acknowledgements

The authors are grateful to Jim Norem and Al Moretti for extensive discussions and for sharing of their experimental data. The authors also wish to thank R.C. Fernow and A. Woodhead for reading the paper and making useful suggestions. Finally, thanks to X. Chang for his assistance with the PARMELA code. This work was supported by the US Department of Energy, Contract no. DE-AC02-98CH10886.

References

[1] R.B. Palmer, J.S. Berg, R.C. Fernow, J.C. Gallardo, H.G. Kirk, Y. Alexahin, D.V. Neuffer, S.A. Kahn, D.J. Summers, in: Proceedings of the 2007 Particle Accelerator Conference, 2007, p. 3193.

[2] M. Apollonio, J.S. Berg, A. Blondel, A. Bogacz, S. Brooks, J.-E. Campagne, D. Caspar, C. Cevata, P. Chimenti, J. Cobb, M. Dracos, R. Edgecock, I. Efthymiopoulos, A. Fabich, R. Fernow, F. Filthaut, J. Gallardo, R. Garoby, S. Geer, F. Gerigk, G. Hanson, R. Johnson, C. Johnstone, D. Kaplan, E. Keil, H. Kirk, A. Klier, A. Kurup, J. Lettry, K. Long, S. Machida, K. McDonald, F. Méot, Y. Mori, D. Neuffer, V. Palladino, R. Palmer, K. Paul, A. Poklonskiy, M. Popovic, C. Prior, G. Rees, C. Rossi, T. Rovelli, R. Sandström, R. Sevior, P. Sievers, N. Simos, Y. Torun, M. Vretenar, K. Yoshimura, M.S. Zisman, J. Instrum. 4 (2009) P07001.

[3] C. Johnstone, M. Berz, D. Errede, K. Makino, Nucl. Instr. Meth. Phys. Res. A 519 (2004) 472.

[4] R.C. Fernow, R.B. Palmer, Phys. Rev. ST Accel. Beams 10 (2007) 064001.

[5] C.J. Johnstone, A. Bross, I. Rakhno, in: Proceedings of the 2005 Particle Accelerator Conference, Knoxville, TN, 2003, p. 3482.

[6] A. Moretti, Z. Qian, J. Norem, Y. Torun, D. Li, M. Zisman, Phys. Rev. ST Accel. Beams 10 (2005) 072001.

[7] K.L. Jensen, Y.Y. Lau, D.W. Feldman, P.G. O'Shea, Phys. Rev. ST Accel. Beams ST 11 (2008) 081001.

[8] C.A. Brau, AIP Conf. Proc. 413 (1997) 278.

[9] Y.Y. Lau, D.G. Colombant, M. Pilloff, J. Appl. Phys. 70 (1991) 4.

[10] R.B. Palmer, R.C. Fernow, J.C. Gallardo, D. Stratakis, D. Li, Phys. Rev. ST Accel. Beams 12 (2009) 031002.

[11] G.S. Nusinovich, AIP Conf. Proc. 1086 (2009) 38;
[] V.A. Dolgashev, S.G. Tantawi, AIP Conf. Proc. 691 (2009) 151.

[12] P.B. Wilson, in: Proceedings of the 2003 Particle Accelerator Conference, 2003, p. 1282.

[13] G.S. Nusinovich, D. Kashyn, T.M. Antonsen Jr., Phys. Rev. ST 12 (2009) 101001.

[14] A. Broos, M. Ellis, S. Geer, O. Mena, S. Pascoli, Phys. Rev. D. 77 (2008) 093012.

[15] J. Norem, V. Wu, A. Moretti, M. Popovic, Z. Qian, Y. Torun, N. Solomey, Phys. Rev. ST Accel. Beams 6 (2003) 072001.

[16] R. Fowler, L. Nordheim, Proc. R. Soc. A 119 (1928) 173.

[17] M. Neubauer, Surface analysis to electrodes before and after 800 MHz breakdown test, in: Presentation at the 2009 Muon Collider Task Force Meeting, https://mctf.fnal.gov/meetings/2009/01_08/surface_analysis_of_electrodes_before_and_after_mta.ppt/view.

[18] W.R. Smythe, in: Static and Dynamic Electricity, McGraw-Hill, New York, 1950.

[19] J.C. Gallardo, D. Stratakis, 2008, to be published.

[20] D. Li, J. Corlett, R. MacGill et al., in: Proceedings of the EPAC 2002, Paris, France, 2002, p. 2160.

[21] L. Young, J. Billen, in: Proceedings of the 2003 Particle Accelerator Conference, 2003, p. 3521.

[22] J.H. Billen, L. Young, in: Proceedings of the 1993 Particle Accelerator Conference, 1993, p. 790.

[23] Lockwood, G.J., Ruggles, L.E., Miller, G.H., Halbleib, J.A., Calorimetric measurement of electron energy deposition in extended media: theory vs experiment, Sandia Labs Report, SAND 79-0414.27, 1980.

[24] D. Stratakis, J.S. Berg, J.C. Gallardo, R.B. Palmer, in: Proceedings of the 2009 Particle Accelerator Conference, TU5PFP004, 2009.

[25] J.V. Beck, K.D. Cole, A. Haji-Sheikh, B. Litkouhi, in: Heat Conduction Using Green's Functions, Hemisphere Publishing Corporation, 1992.

[26] See Eq. X20.1 and Eq. R00.1a in Ref. 25.

[27] S.G. Tantawi et al., in: Proceedings of PAC07, Albuquerque, New Mexico, USA, p. 2370.

[28] D.P. Pritzkau, R.H. Siemann, Phys. Rev. ST Accel. Beams 5 (2002) 112002.

[29] O.A. Nezhevenko, V.P. Yakovlev, J.L. Hirshfield, G.V. Serdobintsev, in: Proceedings of the 2003 Particle Accelerator Conference, Portland, OR, 2003, p. 2881.

[30] H.M. Musal, Jr., Laser induced damage in optical materials, 1979, NBS Special Publication no. 568 (US GPO Washington, DC, 1980, p. 159.

[31] G. Arnau-Izquierdo, S. Calatroni, S. Heikkinen et al., in: Proceedings of PAC07, Albuquerque, New Mexico, USA, p. 2197.

[32] S.V. Kuzikov, M.E. Plotkin, Int. J. Infrared Milli Waves 29 (2008) 298.